

An Automated Surface Defect Inspection System Using Local Binary Patterns and Co-Occurrence Matrix Textures based on SVM Classifier

Jafar J. Abukhait

Department of Communication, Electronics and Computer Engineering, Tafila Technical University, Tafila, Jordan
e-mail: jafar@ttu.edu.jo

Received: March 3, 2018

Accepted: March 31, 2018

Abstract— Computer vision techniques have been widely used in automating the surface defect inspection process where the goal is to detect and identify defects. Surface defect is defined as global color deviation or local textural irregularity which has the main concern in the inspection process. In this paper, the proposed automated system identifies different surface defects using Support Vector Machine (SVM) classifier according to surface textural features. The proposed system introduces a novel feature description technique that extracts local and global features of surfaces. This technique combines Local Binary Pattern (LBP) features with the global textural features of Gray-level Co-occurrence Matrix (GLCM) to address different surface defects. The proposed system has been tested on wood and ceramic tiles images. Experimental results successfully demonstrated the efficiency of the feature description technique and the overall surface defect inspection system.

Keywords— Co-occurrence matrix, local binary pattern, support vector machine, surface inspection.

I. INTRODUCTION

Automated Surface Inspection (ASI) has been widely adopted in the industry sector in the last two decades to detect defect regions on surfaces or to identify the defect type and its existence on the surface. Surface defect is defined as local textural irregularities; or global deviation of color which is known as a shade or tonality problem [1]. Automated Surface Inspection (ASI) of wood, steel, textile and ceramic tiles is an alternate of human visual inspection, where a real-time feedback is required when a certain defect occurs because of labor costs and human distraction that affect the decision.

Detection of textural defects is the main concern of researchers. These defects can be categorized into different types and names according to the shape of textural irregularity and the surface material. Spot regions such as wood knots, ceramic tiles blobs and lengthwise breakage or separation, wood checks and ceramic tiles cracks are the most common defects of surfaces [2], [3]. Fig. 1 shows different types of defects on wood and ceramic tiles surfaces.

In this paper, an automated system is proposed to recognize different surface defects using Support Vector Machine (SVM) classifier according to surface textural features. It has the ability to recognize wood checks and knots, as well as ceramic tiles cracks and blobs. The proposed system introduces a feature description technique that extracts local and global features of surfaces. This technique combines Local Binary Pattern features with the global textural features of Gray-level Co-occurrence Matrix to address different types of surface defects. The proposed system can be deployed in the industrial sector instead of the human surface inspection for labor cost and the distraction which could affect the human decision.

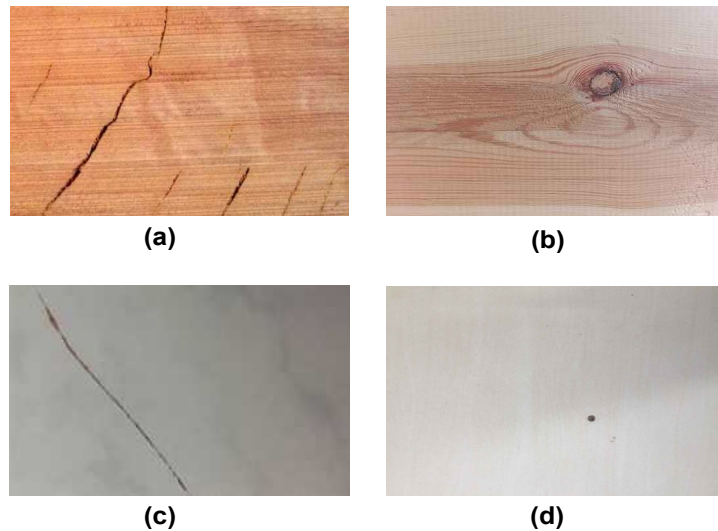


Fig. 1. Examples of surface defects: a) wood check, b) wood knot, c) ceramic tile crack, d) ceramic tile blob

II. PREVIOUS WORKS

There are numerous reported works in the past two decades during which computer vision based surface inspection has become one of the most important application areas. The feature extraction techniques used to inspect surface textural irregularities have the main influence on the overall accuracy of the defect detection and identification. These techniques can be categorized into: statistical approaches, structural approaches, and filter-based approaches [1]-[19].

Statistical approaches, which rely on measuring the spatial distribution of pixel, have been used to extract surface features in the inspection process. These approaches are based on: histogram properties, co-occurrence matrix, and local binary pattern. In [2], a flaw detection technique and defect classification algorithm based on pixels intensity and contrast have been applied on flat and textured ceramic tiles to identify several defects. This technique has more computations and less efficiency. In [6], the textural features extracted from the co-occurrence matrix have been used to detect surface defects. Co-occurrence matrix features have been used also to detect defects on textile and thin-film transistor (TFT) array surfaces [13], [14]. The efficiency of co-occurrence matrix technique is small. A local binary pattern has been deployed in many works to detect surface, wood, and pavement defects [8]-[11]. Only local textural irregularities have been detected.

Structural approaches, which are based on edge features and morphological operation, have been used by many researchers. In [5], a set of morphological techniques along with intensity adjustment, histogram equalization and noise reduction techniques has been deployed on tiles to detect several defects. Blob measurements such as size, perimeter, and spatial distribution have been used with k-means clustering in [16], [18]. In [17], morphological operations have been used to detect fabric defects. These morphological techniques are time consuming.

Filter-based approaches, which are based on spatial and frequency-domain filters, have been used in many works for surface inspection. In [4], combined texture features have been extracted from ceramic tile images before deploying back propagation neural network to detect existing defects. The combined features used are based on undecimated discrete wavelet transform and co-occurrence matrix. In [7], [12], a defect detection algorithm using Gabor wavelet and Gaussian filter has been proposed. In [19], a vision-based inspection system was proposed to identify seven defects on metal surfaces. The proposed system used a

two-level DWT decomposition and Fourier spectral to compute texture. These techniques are suitable for low level intensity defects.

III. MATHEMATICAL BACKGROUND

A) Gray Level Co-occurrence Matrix (GLCM)

The gray level co-occurrence matrix (GLCM), as proposed in [20], was used to calculate the features of various defects, which can serve as basis for defect recognition. GLCM of an image is defined as the distribution of co-occurring gray levels at a given offset: direction (θ) and distance (d). The relative frequencies of two neighboring pixels, one with gray level i and the other with gray level j , are calculated from the scaled image to construct the co-occurrence matrix P_{ij} . This co-occurrence matrix (P_{ij}) can be calculated with different values of d such as: 1, 2, and 3; and different values of θ such as: 0, 45, 90, and 135 as shown in Fig. 2.

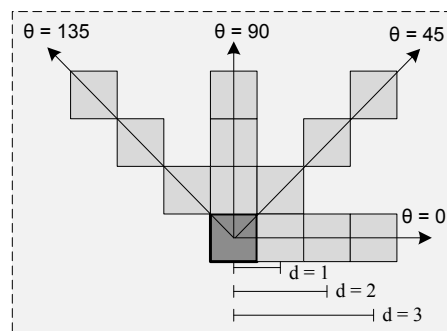


Fig. 2. GLCM with different offsets.

A variety of textural features can be extracted from the co-occurrence matrix P_{ij} such as: Energy, Contrast, Correlation, Homogeneity, Entropy, Autocorrelation, Dissimilarity, and Cluster Shade [22]. These features can be used as a descriptor of the original image. The following equations define a set of these features given that: $p(i,j)$ is the $(i,j)^{\text{th}}$ element in the co-occurrence matrix; μ_x and μ_y are the mean values for both the rows and columns of the matrix; σ_x and σ_y are the standard deviation values for both the rows and columns of the matrix; and N_g is the number of gray levels in the scaled image [20]-[22]:

$$\mu_x = \sum_i \sum_j i \cdot p(i, j) \quad (1)$$

$$\mu_y = \sum_i \sum_j j \cdot p(i, j) \quad (2)$$

$$\sigma_x = \sum_i \sum_j (i - \mu_x)^2 \cdot p(i, j) \quad (3)$$

$$\sigma_y = \sum_i \sum_j (j - \mu_y)^2 \cdot p(i, j) \quad (4)$$

The textural features are defined as shown in (5)-(12) [20]-[22]:

1) Energy

$$f_1 = \sum_i \sum_j p(i, j)^2 \quad (5)$$

2) Contrast

$$f_2 = \sum_{n=0}^{N_g-1} n^2 \left\{ \sum_{i=1}^{N_g} \sum_{\substack{j=1 \\ |i-j|=n}}^{N_g} p(i, j) \right\} \quad (6)$$

3) Correlation

$$f_3 = \frac{\sum_i \sum_j (ij)p(i, j) - \mu_x \mu_y}{\sigma_x \sigma_y}. \quad (7)$$

4) Homogeneity

$$f_4 = \sum_i \sum_j \frac{1}{1+(i-j)^2} p(i, j) \quad (8)$$

5) Entropy

$$f_5 = - \sum_i \sum_j p(i, j) \log(p(i, j)) \quad (9)$$

6) Autocorrelation

$$f_6 = \sum_i \sum_j (ij) \cdot p(i, j) \quad (10)$$

7) Dissimilarity

$$f_7 = \sum_i \sum_j |i - j| \cdot p(i, j) \quad (11)$$

8) Cluster Shade

$$f_8 = \sum_i \sum_j (i + j - \mu_x - \mu_y)^3 \cdot p(i, j) \quad (12)$$

B) Local Binary Pattern (LBP)

Local Binary Pattern (LBP), as proposed in [23], [24], is a gray-scale and rotation-invariant operator used to extract local texture features of an image. In order to compute the LBP for a given pixel position (x_c, y_c) , a comparison is made between the pixel value and its surrounding pixel intensities. If the value of the surrounding pixel is greater than the center pixel value, the surrounding pixel is marked as 1; otherwise, it is marked as 0. The number of surrounding pixels can be 4, 8, 12, 16, or 24 as shown in Fig. 3. Using eight surrounding pixels would yield an 8-bit binary code, which is assigned as the new pixel value of the centered pixel as shown in Fig. 4.

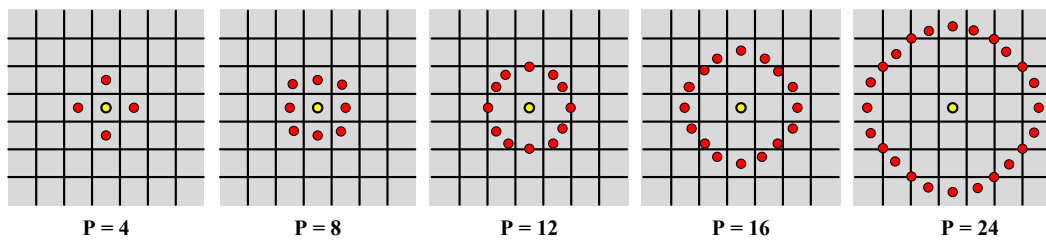


Fig. 3. Circularly symmetric surrounding sets for LBP

The formula of LBP can be expressed as:

$$LBP_p(X_c, Y_c) = \sum_{p=0}^{P-1} S(g_p - g_c) 2^p \quad (13)$$

Where g_c corresponds to the gray value of the centered pixel; g_p corresponds to the gray value of neighboring pixels; P is the number of surrounding pixels; and S is a function defined as:

$$S(x) = \begin{cases} 0, & x < 0 \\ 1, & x \geq 0 \end{cases} \tag{14}$$

The LBP_p operator produces 2^P different local binary patterns. To make local binary patterns invariant to rotation, a new definition of LBP is represented:

$$LBP_p^{ri} = \min\{ROR(LBP_p, i) \mid i = 0, 1, \dots, P - 1\} \tag{15}$$

where $ROR(x, i)$ performs a circular bit-wise right shift on the P -bit number i times; and it thus achieves 36 unique rotation invariant local binary patterns in case of LBP_p . These local binary patterns describe bright spots, dark spots, and edges as mentioned in [8].

An improved edition of LBP is introduced in [23] which adopts a uniformity measure (U) defined as the number of spatial transitions (bitwise 0/1 changes) in the local binary pattern. For example, pattern 1111111_2 has U value of 0, whereas pattern 0001111_2 has U value of 2. This uniformity measure categorizes local binary patterns to ‘uniform’ patterns (which are fundamental properties of texture and have U value of at most 2) and ‘nonuniform’ patterns. The formula of LBP would be expressed as:

$$LBP_p^{riu2} = \begin{cases} \sum_{p=0}^{P-1} S(g_p - g_c) & \text{if } U(LBP_p) \leq 2 \\ P + 1 & \text{otherwise} \end{cases} \tag{16}$$

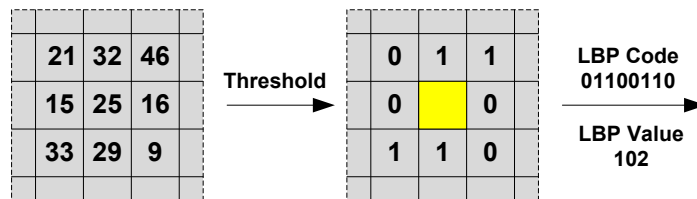


Fig. 4. Schematic of LBP with eight pixel surroundings

This definition would produce $P+1$ uniform patterns and 1 nonuniform pattern. The nonuniform pattern collects all patterns that have $U > 2$. The number of LBP patterns has been reduced to $P+2$ patterns.

The histogram of LBP patterns accumulated over a surface image is used as the feature descriptor of a surface texture. In [23], researchers concluded that the histogram of the uniform patterns has better discrimination results in comparison with histograms of other LBP patterns.

C) Support Vector Machine (SVM)

Support vector machine (SVM) is a linear classifier that deploys statistical learning theory and kernel function for classification. SVM with a sigmoid kernel function is similar to a two-layer feed forward neural network response. SVM is more efficient than the neural network in solving complex problems with a large data set and high dimensionality to avoid overfitting [25]-[27]. The concept of SVM suggests the optimal hyperplane that maximizes the margin between the hyperplane itself and the closest vectors belonging to both classes. Fig. 5 shows an optimal hyperplane that separates the classes with a maximum margin [27]-[29].

In a case, input space is: $\{x_1, x_2, x_3, \dots, x_n\}$; and output space is: $y \in \{-1, 1\}$. The hyperplane separating the two classes can be represented by [27]-[29]:

$$\vec{w} \cdot \vec{x} + b = 0 \tag{17}$$

where w (weight) is the orthogonal vector to the hyperplane determining its orientation; and b (bias) is the distance from the origin to the hyperplane.

Any training sample should satisfy:

$$\vec{w} \cdot \vec{x} + b \geq 1 \text{ for } y = +1 \tag{18}$$

$$\vec{w} \cdot \vec{x} + b \leq -1 \text{ for } y = -1 \tag{19}$$

These two inequalities can be combined to get:

$$y(\vec{w} \cdot \vec{x} + b) - 1 \geq 0 \tag{20}$$

The formulation of this problem would be:

$$\text{maximize } \frac{2}{\|\vec{w}\|} \text{ or minimize } \frac{1}{2} \|\vec{w}\|^2 \tag{21}$$

Such that: $y(\vec{w} \cdot \vec{x} + b) - 1 \geq 0$

To solve this optimization problem, a Lagrange multiplier is suggested; and the problem becomes:

$$\text{minimize } L_p \equiv \frac{1}{2} \|\vec{w}\|^2 - \sum_{i=1}^1 \alpha_i y_i (\vec{w} \cdot \vec{x}_i + b) + \sum_{i=1}^1 \alpha_i \tag{22}$$

Such that $\alpha_i \geq 0$ where α is the Lagrange multiplier.

The result of solving SVM with Lagrange is a decision function in terms of Lagrange multipliers α and bias (b) for test input x_t :

$$y_t = \sum_{i=1}^1 \alpha_i y_i < \vec{x}_t \cdot \vec{x}_i > + b \tag{23}$$

If data is not linearly separable, Slack variables ξ_i can be added to allow mis-classification of difficult or noisy data points. The formulation would be:

$$\text{minimize } \frac{1}{2} \|\vec{w}\|^2 + C \sum_{i=1}^n \xi_i \tag{24}$$

where C is a cost function with $y_i (\vec{w}^T \vec{x}_i + b) \geq 1 - \xi_i$ and $\xi_i \geq 0$

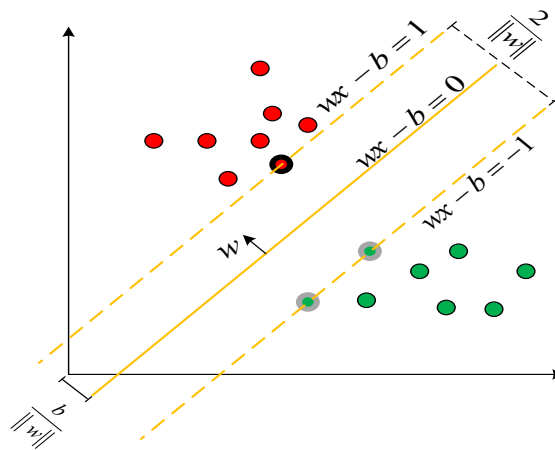


Fig. 5. SVM optimal hyperplane example

IV. SURFACE DEFECT INSPECTION SYSTEM

The surface inspection system, as shown in Fig. 6, consists of two stages:

- Feature Description: in which a feature descriptor of surface images is constructed by combining the histogram of a local binary pattern image and the textural features extracted from the gray level co-occurrence matrix.
- Classification Model Construction: in which a linear support vector machine classifier is trained on the previous feature descriptors of images with defect-free and defective surfaces.

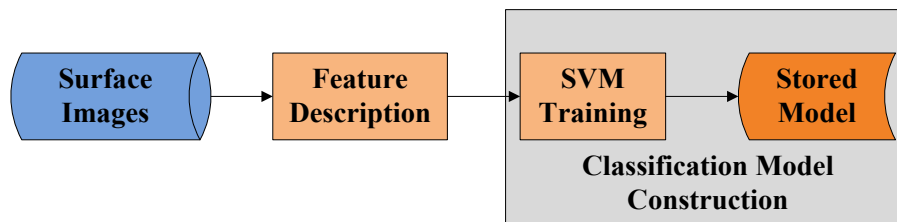


Fig. 6. Diagram of the surface inspection system

A) Feature Description

This stage consists of two modules as shown in Fig. 7: Local Binary Pattern (LBP) module and Gray-level Co-occurrence Matrix (GLCM) module. The input of each module is a gray scale surface image, while the output of each module is a feature descriptor of the surface image. Both feature descriptors extracted from the two modules are combined and concatenated to construct one feature descriptor that describes shape and pattern details of the surface image. This combining process has been fulfilled to achieve the local features from LBP and global features from GLCM which yield an efficient descriptor of surface images.

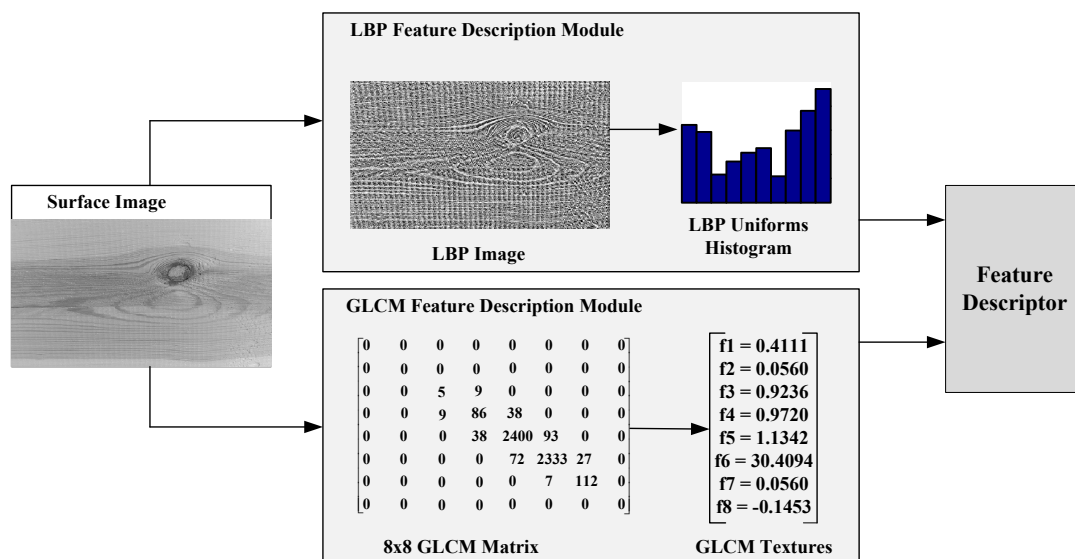


Fig. 7. Feature description

A.1. LBP Feature Description Module

This module generates a feature vector by applying the LBP operator on the surface image. A rotation-invariant LBP with eight pixel surroundings has been deployed on each surface

image to generate a LBP image which describes bright spots, dark spots, and edges. The formula of LBP with eight surroundings can be expressed as:

$$LBP_8(X_c, Y_c) = \sum_{p=0}^7 S(g_p - g_c) 2^p \quad (25)$$

Where g_c corresponds to the gray value of the centered pixel; g_p corresponds to the gray value of neighboring pixels; and S is a function defined as:

$$S(x) = \begin{cases} 0, & x < 0 \\ 1, & x \geq 0 \end{cases} \quad (26)$$

With rotation-invariance operator, the previous formula becomes:

$$LBP_8^{ri} = \min\{ROR(LBP_8, i) \mid i = 0, 1, \dots, 7\} \quad (27)$$

where $ROR(x, i)$ performs a circular bit-wise right shift on the 8-bit number i times. It thus achieves 36 unique rotation invariant LBP patterns instead of the original 256 LBP patterns. Applying the uniformity measure (U), LBP patterns would be categorized into 'Uniform' patterns and 'Non-uniform' ones. The formula of LBP with a uniformity measure would be expressed as:

$$LBP_8^{riu2} = \begin{cases} \frac{\sum_{p=0}^7 S(g_p - g_c)}{9} & \text{if } U(LBP_8) \leq 2 \\ \text{otherwise} & \end{cases} \quad (28)$$

This definition would produce nine uniform patterns and one Non-uniform pattern as shown in Fig. 8. The final step in this stage is to compute the histogram of LBP uniform patterns. This histogram would have ten bins including nine uniform patterns and one bin for all other Non-uniform patterns.

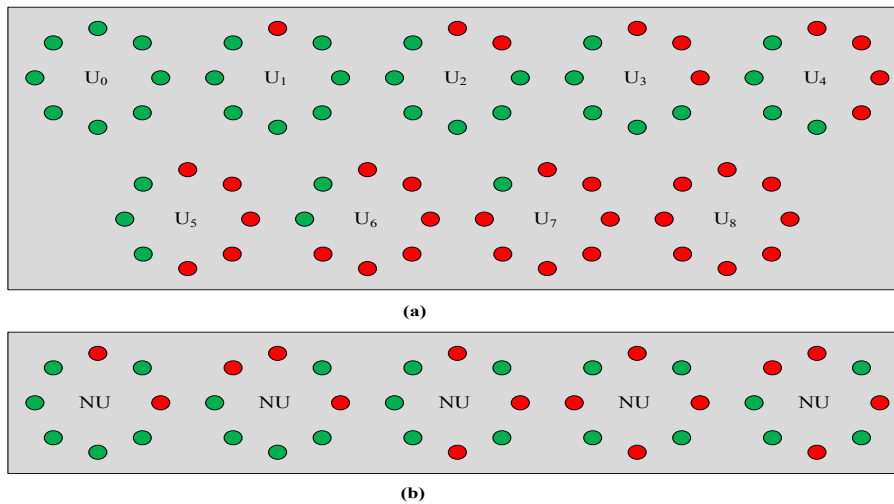


Fig. 8. Examples of LBP_8 patterns: a) the nine uniform patterns. b) examples of non-uniform patterns

A.2. GLCM Feature Description Module

This module generates a feature vector by computing the GLCM on the surface image. The surface image is initially scaled to eight gray levels, before the co-occurrence matrix P_{ij} is computed with direction ($\theta = 0^\circ$) and distance ($d = 1$). Eight textural features are extracted from the co-occurrence matrix P_{ij} . These eight features are: Energy (f_1), Contrast (f_2), Correlation (f_3), Homogeneity (f_4), Entropy (f_5), Autocorrelation (f_6), Dissimilarity (f_7), and Cluster Shade (f_8). Finally, a feature vector of GLCM is constructed from such features as:

Feature Vector of GLCM=[f1, f2, f3, f4, f5, f6, f7, f8]

Finally in this stage, a feature descriptor of length 18 is constructed by combining the ten histogram pins of LBPs (nine uniform LBPs and one non-uniform LBP) and the eight textural features of GLCM. The format of the feature vector would be:

Feature Descriptor=[U0, U1, U2, U3, U4, U5, U6, U7, U8, NU, f1, f2, f3, f4, f5, f6, f7, f8]

B) Classification Model Construction

This stage constructs two classification models for each surface based on the feature descriptors produced in the previous stage. Linear SVM is trained on defect-free and defective surface images, after producing their feature descriptors, to build up a ternary-class classification model as shown in Fig. 9. The output of this stage is two classification models: one for ceramic tiles classification, and the other for wood classification. Each model is trained in a one-versus-other fashion to generate a ternary-class structure representing the state of the surface which is either defect-free or with two different types of defects.

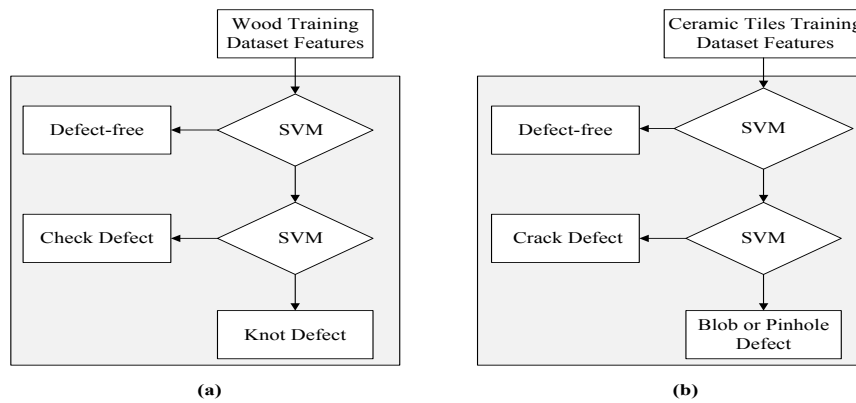


Fig. 9. Classification model construction: a) wood surfaces model, b) ceramic tiles surfaces model

Each model is constructed by training it twice. The optimal hyperplane in each time maximizes the margin between the hyperplane itself and the closest vectors belonging to both classes.

In a case, feature descriptors of the trained images dataset are: $\{x_1, x_2, x_3, \dots, x_n\}$; and output label is: $y \in \{-1, 1\}$.

The hyperplane separating the two classes can be represented by:

$$\vec{w} \cdot \vec{x} + b = 0 \tag{29}$$

where w (weight) is the orthogonal vector to the hyperplane determining its orientation; and b (bias) is the distance from the origin to the hyperplane.

To solve this optimization problem, a Lagrange multiplier (α) is suggested. The result of solving SVM with Lagrange is a decision function in terms of Lagrange multipliers and bias (b) for test input x_t as follows:

$$y_t = \sum_{i=1}^l \alpha_i y_i < \vec{x}_i, \vec{x}_t > + b \tag{30}$$

V. EXPERIMENTAL RESULTS

The proposed surface defect inspection system has been validated on wood and ceramic tiles images. These surface images have been captured using SAMSUNG ST65 camera and scaled to 320 x 240 pixels by a numeric fraction to overcome the impact of objects' distortion. The proposed surface defect inspection system has been implemented in MATLAB software running on 2.4-GHz i3 CPU.

A dataset of 414 surface images has been collected to be used in both the training and testing phases. This dataset includes ceramic tiles and wood images. In addition, it has defect-free and defective surface images. Table 1 shows the exact division of dataset images. These dataset images have been categorized by a human expert to: defect-free, crack defect, and blob or pinhole defect for ceramic tiles; and to: defect-free, check defect, and knot defect for wood surfaces. Crack, Pinhole, and Blob defects of 35 ceramic tiles were enforced by manual manipulation of surface images to compensate for the lack of enough number of raw images that satisfy these defects.

TABLE 1
SURFACE IMAGES DATASET DIVISION

Defect \ Surface	Ceramic Tiles	Wood
Blob or Pinhole/Knot Defects	42	58
Crack/Check Defects	32	34
Defect-free	124	124
Total Surface Images	198	216
Total Dataset Images	414	

A feature descriptor of each surface image in the dataset is extracted and represented by this feature descriptor. This descriptor has been achieved by combining the histogram of uniform LBP patterns with the eight textural features computed from the GLCM. Fig. 10 shows examples of defect-free and defective wood surfaces along with the features obtained from both LBP Uniforms histogram and GLCM textural features. Fig. 11 shows examples of defect-free and defective ceramic tiles surfaces along with the features obtained from both LBP Uniforms histogram and GLCM textural features.

The proposed surface inspection system has been validated by training and testing it twice on ceramic tiles and wood images. Table 2 shows the number and categories of the training data used.

TABLE 2
THE NUMBER OF SURFACE IMAGES' CATEGORIES USED IN THE TRAINING PHASE

Defect \ Surface	Ceramic Tiles	Wood
Blob or Pinhole/Knot Defects	30	40
Crack/Check Defects	20	20
Defect-free	50	70
Total Surface Images	100	130
Total Dataset Images	230	

The proposed surface inspection system has been tested on 184 surface images (98 of ceramic tiles and 86 of wood images). The decision of the proposed system has been compared with

the dataset categorized by a human expert in the data collection step. Table 3 shows the decisions of the proposed inspection system.

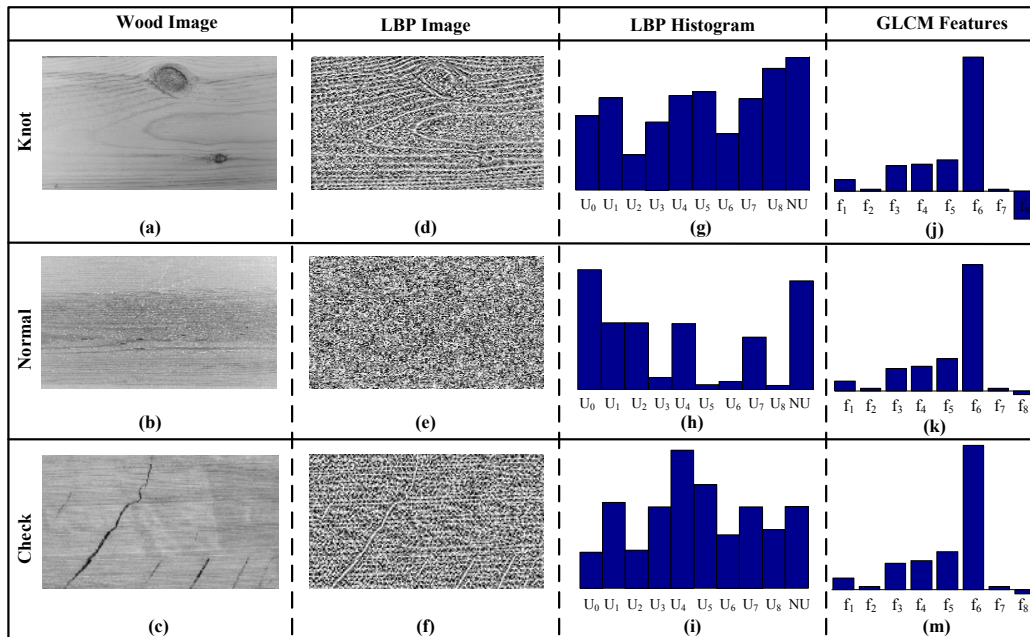


Fig. 10. Examples of feature description results of wood surfaces: a-c) original images, d-f) LBP images, g-i) LBP uniform histograms, j-m) GLCM textural features

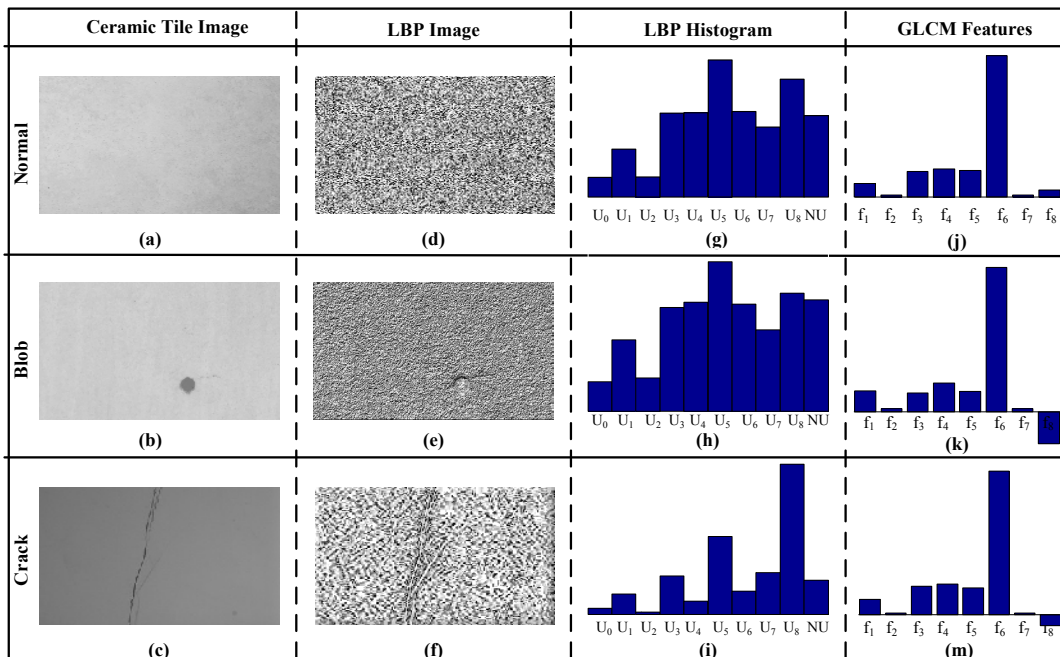


Fig. 11. Examples of feature description results of ceramic tiles surfaces: a-c) original images, d-f) LBP images, g-i) LBP uniform histograms, j-m) GLCM textural features

TABLE 3
THE ACCURACY OF THE PROPOSED SYSTEM ON CERAMIC TILES AND WOOD SURFACES

	Ceramic Tiles	Wood	Both Surfaces
Total Number of Tested Surfaces	98	86	184
Number of Surfaces Identified Correctly	95	81	176
Number of Surfaces Identified Falsely	3	5	8
Accuracy	96.9%	94%	95.6%

The comparison shows a true decision of the inspection system on 176 surface images while 8 surface images have been identified falsely. The accuracy of the inspection system is 96.9% for the ceramic tile images and 94% for the wood images. This accuracy difference between the two surfaces is due to the complex and non-uniform patterns on wood surfaces. The overall accuracy of the proposed system on both surfaces was 95.6%.

The proposed system has been compared to other state-of-the-art surface defect inspection systems based on three parameters: number of classes, surface types, and accuracy. The proposed system outperformed other systems based on accuracy as shown in Table 4. In addition, the proposed system has been tested on two different surfaces, whereas most systems in the literature are tested on one surface type.

TABLE 4
COMPARISON OF THE PROPOSED SYSTEM WITH STATE-OF-THE-ART SYSTEMS

	DWT-Fourier Spectral-SVM [19]	GLCM-FFNN [14]	LBP-BPNN [9]	UDWT-GLCM-BBNN [4]	GLCM-BPNN [13]	Proposed System
Number of Classes	7	2	3	2	5	3
Surface Type	Reflected Metal	Textile	Wood	Ceramic Tiles	TFT Array	Wood and Ceramic Tiles
Accuracy (%)	85	91	93.3	93.2	83.3	95.6

VI. DISCUSSIONS AND CONCLUSIONS

In this paper, we have proposed an automated system for surface inspection to label a given surface either as defective or defect-free. The proposed inspection system has combined both LBP uniform patterns histogram and GLCM textural features to construct powerful and discriminative feature descriptors of surfaces. Linear SVM classifier has been deployed to build up the classification model. The proposed system has been validated on wood and ceramic tile images; and it showed efficient and promising accuracy results.

The system can be enhanced in the future by considering: 1) Classifying surfaces to multi-classes; 2) considering more features of LBP and GLCM in the proposed system; 3) testing the proposed system on other surfaces and other types of ceramic tiles; and 4) adapting gray scale defects in addition to shape and textural defects discussed in this paper.

REFERENCES

- [1] X. Xie, "A review of recent advances in surface defect detection using texture analysis techniques," *Computer Vision and Image Analysis*, vol. 7, no. 3, pp. 1-22, 2008.

- [2] Md. Islam, Md. Sahriar and Md. Hossain, "An enhanced automatic surface and structural flaw inspection and categorization using image processing both for flat and textured ceramic tiles," *International Journal of Computer Applications*, vol. 48, no. 3, pp. 975-888, 2012.
- [3] R. Conners, C. Mcmillin, K. Lin and R. Vasquez-Espinosa, "Identifying and locating surface defects in wood: part of an automated lumber processing system," *IEEE Transactions on Pattern Analysis and Machine Intelligence*, vol. PAMI-5, no. 6, pp. 573-583, 1983.
- [4] A. Fathi, A. Monadjemi and F. Mahmoudi, "Defect detection of tiles with combined undecimated wavelet transform and GLCM features," *Soft Computing and Engineering*, vol. 2, no. 2, pp. 2231-2307, 2012.
- [5] H. Elbehery, A. Henfnawy and M. Elewa, "Surface defect detection of ceramic tiles using image processing and morphological operation," *Proceedings of the World Academy of Science, Engineering and Technology*, vol. 5, pp. 158-162, 2005.
- [6] M. Sharma and G. Kaur, "Integrated approach for defect detection in ceramic tiles," *Computer and Technology*, vol. 3, no. 2, pp. 259-262, 2012.
- [7] K. Sivabalan, D. Gnanadurai, "Efficient defect detection algorithm for gray level digital images using Gabor wavelet filter and Gaussian Filter," *Engineering Science and Technology*, vol. 3, no. 4, pp. 3195-3202, 2011.
- [8] Y. Hu and C. Zhao, "A local binary pattern based methods for pavement crack detection," *Pattern Recognition Research*, vol. 5, no. 1, pp. 140-147, 2010.
- [9] Y. Zhang, Y. Zhao, Y. Liu, L. Jiang and Z. Chen, "Identification of wood defects based on LBP features," *Proceedings of Chinese Control Conference*, pp. 4202-4205, 2016.
- [10] S. Fekri-Ershad and F. Tajeripour, "A robust approach for surface defect detection based on one dimensional local binary patterns," *Indian Journal of Science and Technology*, vol. 5, no. 8, pp. 3197-3203, 2012.
- [11] T. Maenpaa, M. Turtinen and M. Pietikainen, "Real-time surface inspection by texture," *Real-Time Imaging*, vol. 9, no. 5, pp. 289-296, 2003.
- [12] C. Tikhe and J. Chitode, "Metal surface inspection for defect detection and classification using Gabor filter," *Computer Applications*, vol. 3, no. 6, pp. 13702-13709, 2014.
- [13] Y. Shih-Wei, L. Chern-Sheng, L. Shir-Kuan and C. Hsien-Te, "Automatic defect recognition of TFT array process using gray level co-occurrence matrix," *Optik-International Journal for Light and Electron Optics*, vol. 125, no. 11, pp. 2671-2676, 2014
- [14] G. Azim, "Identification of textile defects based on GLCM and neural networks," *Computer and Communications*, vol. 3, no. 12, pp. 1-8, 2015.
- [15] V. Mohan and S. Kumar, "An automated tiles defect detection," *Computer Applications*, vol. 109, no. 11, pp. 24-27, 2015.
- [16] J. Kittler, R. Marik, M. Mirmehdi, M. Petrou and J. Song, "Detection of defects in colour texture surfaces," *Proceedings of IAPR Conference on Machine Vision Applications*, pp. 558-567, 1994.
- [17] B. Mallick-Goswami and A. Datta, "Detecting defects in fabric with laser-based morphological image processing," *Textile Research Journal*, vol. 70, no. 9, pp. 758-762, 2000.

- [18] K. Song, J. Kittler and M. Petrou, "Defect detection in random colour textures," *Image and Vision Computing*, vol. 14, no. 9, pp. 667-683, 1996.
- [19] Z. Xue-wu, D. Yan-qiong, L. Yan-yun, S. Ai-ye and L. Rui-yu, "A vision inspection system for the surface defects of strongly reflected metal based on multi-class SVM," *Expert Systems with Applications*, vol. 38, no. 5, pp. 5930-5939, 2011.
- [20] R. Haralick, K. Shanmugam and I. Dinstein, "Textural features of image classification," *IEEE Transactions on Systems, Man and Cybernetics*, vol. SMC-3, no. 6, pp. 610-621, 1973.
- [21] L. Soh and C. Tsatsoulis, "Texture analysis of SAR sea ice imagery using gray level co-occurrence matrices," *IEEE Transactions on Geoscience and Remote Sensing*, vol. 37, no. 2, pp. 780-795, 1999.
- [22] D. Clausi, "An analysis of co-occurrence texture statistics as a function of grey level quantization," *Canadian Journal of Remote Sensing*, vol. 28, no. 1, pp. 45-62, 2002.
- [23] T. Ojala, M. Pietikainen and T. Maenpaa, "Multiresolution gray-scale and rotation invariant texture classification with local binary patterns," *IEEE Transactions on Pattern Analysis and Machine Intelligence*, vol. 24, no. 7, pp. 971-987, 2002.
- [24] M. Pietikäinen, T. Ojala and Z. Xu, "Rotation-invariant texture classification using feature distributions," *Pattern Recognition*, vol. 33, no. 1, pp. 43-52, 2000.
- [25] B. Scholkopf and A. J. Smola, *Learning with Kernels*, Massachusetts: MIT Press, 2002.
- [26] A. Karatzoglou, T. U. Wien, D. Meyer, W. Wien, K. Hornik and W. Wien, "Support vector machines in R," *Statistical Software*, vol. 15, no. 9, pp. 1-28, 2006.
- [27] C. Burges, "A tutorial on support vector machines for pattern recognition," *Data Mining and Knowledge Discovery*, vol. 2, no. 2, pp. 121-167, 1998.
- [28] N. Cristianini and J. Shawe-Taylor, *An Introduction to Support Vector Machines*, Cambridge University Press, 2000.
- [29] V. Vapnik, *The Nature of Statistical Learning Theory*, Springer-Verlag, 1995.